ADVANCED MATERIAL DISTRIBUTION MEASUREMENT IN MULTIPHASE FLOWS: A CASE STUDY

D. L. George and S. L. Ceccio
Department of Mechanical Engineering and Applied Mechanics
University of Michigan
Ann Arbor, Michigan 48109-2121 USA

T. J. O'Hern, K. A. Shollenberger, and J. R. Torczynski
Engineering Sciences Center
Sandia National Laboratories[1]
Albuquerque, New Mexico 87185-5800 USA

ABSTRACT

A variety of tomographic techniques that have been applied to multiphase flows are described. The methods discussed include electrical impedance tomography (EIT), magnetic resonance imaging (MRI), positron emission tomography (PET), gamma-densitometry tomography (GDT), radiative particle tracking (RDT), X-ray imaging, and acoustic tomography. Also presented is a case study in which measurements were made with EIT and GDT in two-phase flows. Both solid-liquid and gas-liquid flows were examined. EIT and GDT were applied independently to predict mean and spatially resolved phase volume fractions. The results from the two systems compared well.

INTRODUCTION

A dilemma encountered in multiphase flow measurements is that probes or instruments should be placed outside the flow domain so as not to disturb the flow itself, yet phase distributions cannot easily be measured from the flow boundary. Tomography, the technique of imaging plane or volume sections within an object, offers a possible solution, and many different tomographic methods have been applied to the measurement of multiphase flows. Most of these tomographic methods have been derived from devices for medical applications, such as electrical impedance tomography (EIT), magnetic resonance imaging (MRI), and positron emission tomography (PET). Presented here is a brief review of a variety of tomographic techniques and related methods that can be used to determine the spatial distribution of the phases in a multiphase flow. In addition, a case study is presented that compares and evaluates two tomographic methods: EIT and gamma-densitometry tomography (GDT).

[1] Sandia is a multiprogram laboratory operated by Sandia Corporation, a Lockheed Martin Company, for the United States Department of Energy under Contract DE-AC04-94AL85000.

REVIEW OF TOMOGRAPHY METHODS FOR MULTIPHASE FLOWS

Radiation-based Tomography

Many tomographic methods applied to multiphase flows involve radiation, such as neutrons, gamma rays, or x-rays, that are only partially attenuated by the flow. Information about local density or phase distributions can be obtained by measuring attenuation of a radiation beam through the domain or by triangulating the locations of radiation sources within the flow. These methods also have the advantages of being nonintrusive and easily applied to industrial conditions but typically require radiation shielding and other methods of personnel protection. The methods are slow since long counting times are needed to obtain useful statistics, but images of high spatial resolution can be readily reconstructed. The next four subsections describe a variety of radiation-based methods applied to the study of multiphase flows.

Radioactive Particle Tracking (RPT). Radioactive particles can be placed in a multiphase flow and used as Lagrangian flow markers. The particle is designed to be a marker of a particular phase in the flow. For example, neutrally buoyant particles can be used to track a liquid "element" of the continuous phase, or the particle can be one of many in a dispersed solid phase. Lin *et al.* (1985), Larachi *et al.* (1994), and Roy *et al.* (1998) provide detailed descriptions of this technique. The radioactive emissions from the particle are measured

DISCLAIMER

with an array of precisely calibrated detectors. The domain of the flow is divided into a number of volume elements, and the signals from the detectors are used to locate the tracer particle within an element. By tracking the particle as it moves across volume elements, the phase velocity may be determined. By tracking the particle over many hours, the flow within a closed vessel can be accurately mapped. For the method to be effective, the particle must move faithfully with the phase of interest — *e.g.*, a solid tracer particle must have the same density and size as the remainder of the dispersed solid phase.

Positron Emission Tomography (PET). In positron emission tomography (PET), radioisotopes, such as fluorine-18, sodium-22, or gallium-68, are placed in the flow to act as tracers. As an atom of the radioisotope decays, it emits a positron, a particle with the same mass as an electron but opposite charge. The positron travels only a few millimeters in solids or liquids before encountering an electron; the resulting annihilation of the two particles produces two gamma photons of the same energy that travel in opposite directions from the annihilation point along a single axis. Because the entire process of emission, annihilation, and photon travel is nearly instantaneous, the photons can be detected simultaneously by an array of radiation detectors around the flow. Tomographic reconstruction methods can then be used to locate the radioactive tracers and image the phase distribution of the flow.

Parker *et al.* (1993, 1995) describe a PET system with two large, position-sensitive detectors and have presented tests of the system on tagged lubricating oil in a bearing test rig. Using a weighted backprojection method, good images were obtained of the oil distribution along 64 parallel planes in the rig; the time required to obtain the data for a full three-dimensional tomogram was about an hour, whereas two-dimensional projections required about a minute. Similar images were obtained of dough hydraulically extruded into a mold over a 40-minute period. McKee *et al.* (1995) used PET to visualize slurry mixing in a cylindrical vessel, using sand labeled with fluorine-18 as the solid phase. Comparisons of PET solids profiles with data from a local conductivity probe showed qualitative agreement; data acquisition required a period of 30 minutes under steady-state conditions. Even with projected advances in data acquisition, PET is likely to be too slow to be useful in situations with time scales below a few seconds. A variation of PET is positron emission particle tracking, or PEPT (Simons, 1995; Parker *et al.*, 1993 and 1995). PEPT is similar to the RPT method described above. A single tracer is placed in the flow, and the photon emission from the particle is used to triangulate the particle position. Because two orthogonal photons are emitted by the tracer particle, fewer detectors can be used compared to conventional RPT.

Gamma Ray Densitometry Tomography (GDT). Gamma ray tomography, or gamma-densitometry tomography (GDT), uses collimated radiation sources to project photon beams through the region of interest and detection systems to measure the fraction of photons that pass through the region unattenuated. Measurement of the attenuation along many different paths through the domain of interest can be combined with linear tomographic reconstruction methods to produce an image of the phase distribution in the domain. GDT has been used for some time to investigate multiphase flows, and comprehensive reviews are provided by Munshi (1990), Beck *et al.* (1993) and Simons (1995). The spatial resolution of GDT systems can be very fine (< 1 mm). At present, the long data acquisition times of GDT systems (tens of minutes to hours) limits their usefulness to the determination of time-averaged properties. X-ray tomography may also be used in situations where lower-energy photons are acceptable (Dyakowski, 1996, and Torczynski *et al.*, 1997).

X-ray Imaging. A number of medical x-ray systems can be used to image multiphase flows, and real-time images of flows are possible. These images can be digitized and analyzed to obtain bubble volumes, velocities, and population statistics. Yates and Cheesman (1992) describe a system used to investigate gas bubble growth and breakup in fluidized beds. The x-ray source produces pulses coordinated with the imaging system which can acquire full images at 25 frames per second. The offline image processing system has been used to produce silhouettes of gas voids within the solid regime that may be used to obtain local gas volume fractions using a deconvolution technique.

Magnetic Resonance Imaging (MRI)

Magnetic resonance imaging (MRI, otherwise known as nuclear magnetic resonance or NMR) is another tomographic method that has its origins in medicine. In MRI a strong magnetic field is applied to the flow, causing nuclei to emit radio signals by precessing in phase with the field. By applying a magnetic field with known gradients, nuclei in different areas of the field will precess at different frequencies, allowing the positions of the nuclei to be determined. In medical applications the field is tuned to cause resonance of hydrogen nuclei (protons); the same approach can be used in multiphase flows involving water or hydrocarbons.

MRI has been used successfully to measure rheological properties of Couette and Poiseuille flows (Abbott *et al.*, 1991; Altobelli *et al.*, 1991). In the latter study steady-state pipe flows were analyzed for variations in axial fluid velocity and particle concentration; the working fluid was a suspension of polymer particles in SAE gear lubricant. Oil velocity profiles were in agreement with analytical predictions, and particle distributions in suspension flows could be explained in part by known velocity effects and the velocity data. Flow velocities of 10^{-4} to 1 m/s have been measured by MRI with a spatial resolution of 10^{-5} m in turbulent conditions (Kose, 1992). Altobelli and Mondy (1998) have successfully used one-dimensional imaging to measure the settling of glass microbubbles in flotation experiments. The microbubbles were thoroughly mixed with a suspending liquid of glycerol and water in a vertical cylinder. As the glass spheres rose to the top of the suspension over several hours, MRI data were taken continuously to measure the volume fraction axial distributions and phase velocities with time. Measured solids settling functions were in agreement with both existing correlations and kinematic theory. Powell (1998) described an MRI system used to visualize flows of pulp suspensions, including velocity profiles in pipe flows. Generally, the length of time required to obtain data for a single image in MRI is greater than 30 seconds.

Acoustic Tomography

Ultrasound can also be used to probe and image a multiphase flow. Dense liquid-solid flows have been visualized with acoustic holography. Shekarriz *et al.* (1998) describe such a system that has been developed for examining dense particle suspensions. Unlike medical ultrasound imaging systems, the plane that is visualized is perpendicular to the direction of insonification. An acoustic beam is transmitted through the multiphase flow with a liquid bath as a coupling medium. The forward scattered sound is focused onto a free surface and mixed with the sound from a reference transducer that is in phase with the object beam, and the acoustic intensity of the mixed signal is visualized as the surface wave pattern. The free surface becomes a diffraction grating with varying amplitude proportional to the acoustic intensity. The surface is then interrogated with the coherent light of a laser, and the resulting holographic image is captured for processing. The spatial resolution of this system is dependent on the acoustic wavelength of the interrogation beam. For a 5-MHz interrogation beam, an in-plane spatial resolution of < 1 mm is reported with a depth of field of 6 mm (Shekarriz and Brenden, 1995; Shekarriz *et al.*, 1998). Care must be taken to select the appropriate interrogation frequency for the multiphase flow under study.

Electrical Impedance Tomography (EIT)

In recent years the medical community has pioneered the use of electrical impedance tomography (EIT) as a less expensive alternative to conventional medical tomographic systems. A survey of the basics of the method and its application to medical diagnostics is found in the book *Electrical Impedance Tomography*, edited by J. G. Webster (1990). Researchers are now attempting to implement such systems for the study of multiphase flows; Plaskowski *et al.* (1995) describes several potential areas for application of the method. EIT employs measurements of the voltage at the boundary of a test domain to reconstruct the impedance distribution within the domain. For AC electrical conduction with field frequencies on the order of tens of megahertz or lower, the electrical potential within the domain, V, is related to the complex electrical conductivity of the domain, σ, by

$$\nabla \bullet \sigma \nabla V = 0 \tag{1}$$

Current injections and voltage measurements are performed at a finite number of boundary electrodes. If N electrodes are used, the domain can be modeled as an N-port impedance network. The total number of linearly independent voltage measurements, R_N, is then given by

$$R_N = \frac{N(N-1)}{2} \tag{2}$$

Several simplifications are generally employed in EIT, which make it possible to reconstruct the domain using discrete finite element methods. These include the assumption that current travels only in a two-dimensional domain, the simple representation of conductivity by a piecewise constant function, and mathematical models to represent the voltage in the domain. It is also assumed in EIT that the impedance distribution within the domain does not change significantly over time while voltage projections are acquired. As a result, EIT systems must acquire projections rapidly to image most multiphase flows. To reconstruct the image of the domain, a "candidate" representation of the impedance distribution is first constructed. A set of voltage projections is then computed from the candidate distribution. The candidate projections are compared to voltages measured on the boundary during current injection, and their difference is characterized by some error criterion. Finally, the candidate distribution is modified based on the error, and a new set of candidate projections is computed. This process continues until some minimum error criterion is satisfied. EIT reconstruction is an ill-posed problem; consequently, the reconstructed impedance "solution" may not satisfy requirements of existence or continuous dependence on the problem data. *A priori* knowledge of the impedance distribution may be used to aid in restoration, but in most multiphase flows such information may not be readily available.

Dickin *et al.* (1993) and Jones *et al.* (1992, 1993, 1994) report the development of EIT systems implemented for the study of multiphase flows. A recent review is also provided by Ceccio and George (1996). EIT systems have been developed for both conducting and non-conducting mixtures, and the number of electrodes ranges from 8 to 32. Complete projection sets for 12-electrode systems can be acquired over time intervals of milliseconds.

CASE STUDY: VALIDATION OF AN ELECTRICAL IMPEDANCE TOMOGRAPHY SYSTEM

This section presents a series of studies in which an EIT system developed at Sandia National Laboratories (O'Hern *et al.*, 1995; Torczynski *et al.*, 1996a) and a GDT system were simultaneously applied to the same two-phase flows. Since the GDT system has already been successfully applied to multiphase flows (Adkins *et al.*, 1996; Torczynski *et al.*, 1996b; Shollenberger *et al.*, 1997a), it was used to assess the accuracy of the EIT system for two-phase flow measurements. The Sandia EIT system and the tomographic reconstruction method are briefly described, and numerical and experimental validation tests of the reconstruction algorithm are presented. The final sections of this paper describe the experimental conditions of the two-phase flow tests and compare results from EIT and GDT. Both liquid-solid flows and air-water flows are examined, with close attention paid to the length scales of the dispersed phase.

Electrical Impedance Tomography System

A description of the Sandia EIT system is presented in Torczynski *et al.* (1997) and George *et al.* (1998). The system consists of an electrode array, or probe ring; a signal generator; a voltage-controlled current source; multiplexers connecting the probe ring to the current source, ground, and measurement electronics; an instrumentation amplifier and phase sensitive demodulators; and a data acquisition card (Fig. 1). The data acquisition card contains an analog-to-digital converter that measures the demodulated DC signals and a digital controller that can be used to select electrodes for current injection, ground, and measurement. The card also acts as an interface to a PC that operates the entire system. During operation the EIT system injects a controlled current through one electrode, "sinks" a second electrode to ground, and measures voltages at all electrodes relative to ground. The domain is excited with a 50-kHz AC electric field; at 50 kHz, the resistive component of impedance dominates for air-water systems.

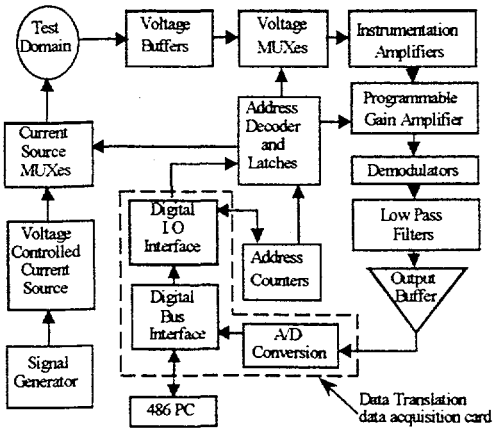

Figure 1. Block diagram of Sandia EIT system.

The voltage signals from each electrode are passed through an amplifier to a phase-sensitive demodulator that separates the signal into two components: one in phase with the EIT carrier signal, the other a quadrature component. These components are low-pass filtered to yield the resistive and capacitive components, respectively, of the measured impedance.

Probe rings were fabricated for use in validation tests and in experiments conducted in a transparent bubble column. Disk electrodes 1.27 cm in diameter and square electrodes 1.27 cm on a side were fabricated from stainless steel. These were mounted at equal azimuthal intervals in Lucite cylinders with an inner diameter of 19.05 cm, a wall thickness of 0.64 cm, and a height of 38.1 cm, twice the inner diameter (Fig. 2a). Another set of electrodes was fashioned from stainless steel strips 0.64 cm wide, 7.62 cm high, and 0.0076 cm thick, mounted in a Lucite cylinder 12.7 cm high (Fig. 2b). While the strip electrodes can in theory produce relatively two-dimensional electric fields, which are easier to model, the point electrodes have higher mechanical integrity and good size-scaling properties. The merits of both types of electrodes were compared during tests and will be discussed in following sections.

The reconstruction algorithm used with the Sandia EIT system has been described in detail by Torczynski *et al.* (1996a, 1997) and is based on the YWT method described by Yorkey *et al.* (1987). In the reconstruction algorithm, the electrical conductivity of the flowing medium is treated as purely resistive (no capacitive contribution), which is reasonable for the air-water systems considered here. The medium is surrounded by an insulating boundary through which current is injected or withdrawn at discrete electrodes. A finite-element method (FEM) representation of the voltage equation is generated, and the electrical conductivity is represented as a function of position and one or more conductivity parameters. To implement the Neumann boundary conditions, current flow is specified everywhere on the boundary (specifically at the electrodes) such that the net current into and out of the domain is zero.

The finite element equations are solved to find both the predicted voltages at the electrodes and the derivatives of the electrode voltages with respect to the conductivity parameters. After the electrode voltages are mapped as functions of the conductivity parameters, a Newton-Raphson algorithm is used to adjust the parameters to minimize the least-squares difference between the computed and

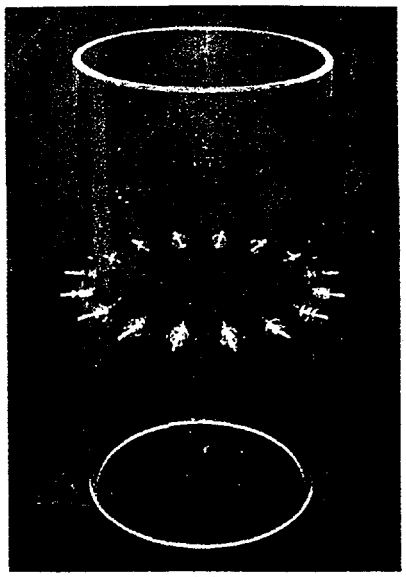

(a)

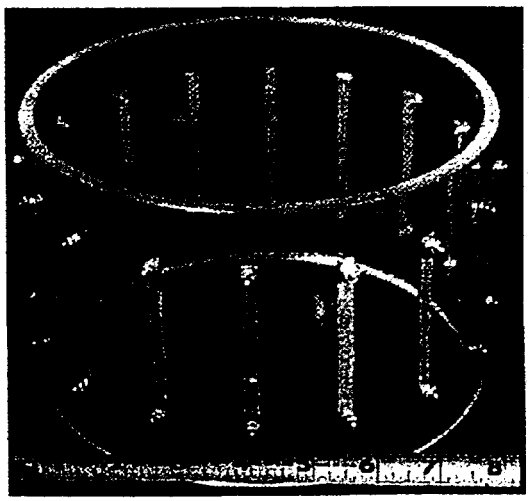

(b)

Figure 2. EIT electrode cylinders: (a) circular point electrodes, (b) strip electrodes. The cylinders have the same diameter; the bottom scale is in inches.

experimental electrode voltages. With the converged parameters, the conductivity distribution can be constructed, and phase information, such as the domain-average gas volume fraction ε_G, can be found from a constitutive model. The two- or three-dimensional Maxwell relation (Maxwell, 1881) is most often used to relate the effective conductivity of the mixture to the gas volume fraction of the mixture.

Separate computer codes have been written to implement this algorithm in two and three dimensions. The two-dimensional code FEMEIT models arbitrary domains, including multiply connected domains and domains with internal probes. Mesh nodes, which are considered to be mathematical points, are used to represent all

electrodes; current-bearing electrodes are modeled as line sources or sinks, extending to infinity out of the plane of the mesh. The global conductivity functions are selected from a library of choices in a subroutine that includes a constant conductivity, a circular insulating region at an arbitrary position, and analytical conductivity distributions. FEMEIT generates and solves the FEM equations using the conductivity library and applies the Newton-Raphson algorithm to determine the final conductivity parameters. For three-dimensional computations the FEM equations are generated and solved using the finite-element code FIDAP (Fluid Dynamics International, 1995). Fundamental FEM solutions have been determined for a range of values of the conductivity shape parameters, and library files have been created that map the electrode voltages in parameter space. To keep the size of the library manageable, only radial variations in the conductivity field are considered. The library file is used with the codes EITCON and EITAXI, which use cubic-spline interpolation and a Newton-Raphson algorithm to determine the final values of the shape parameters. EITCON solves for the gas volume fraction ε_G by assuming a uniform conductivity across the domain, whereas EITAXI solves for coefficients of other conductivity distributions that can be described by the parameters, such as a second- or fourth-order conductivity profile, or a cylindrical insulating inclusion centered in the domain. The reconstruction algorithms have been validated using both analytically and physically derived projection sets. The complete system was also validated with the detection of a series of inclusions in the test domain. These results have been reported in Torczynski *et al.* (1996a, 1997).

Gamma-Densitometry Tomography System

A gamma-densitometry tomography (GDT) system was developed at Sandia for studies of industrial-scale multiphase flows (Torczynski *et al.*, 1996b; Shollenberger *et al.*, 1997a). The GDT system, shown in Fig. 3, employs a 5-curie ^{137}Cs gamma source, a sodium-iodide scintillation detector system, a computer-controlled traverse to position the source and detector, and data acquisition hardware and software. Measurements of gamma-ray attenuation along many different beam paths are translated into a gamma attenuation coefficient, μ, averaged along each path. Attenuation by the testbed walls is subtracted from this raw data, then the time-averaged gas volume fraction distribution in the domain is reconstructed using the Abel transform — *e.g.*, Vest (1985) — and the assumption of an axisymmetric phase distribution, which is reasonable for these experiments.

Experimental Measurements of Two-Phase Flows

The EIT system was applied to *in situ* measurement of two-phase flows. Both liquid-solid and gas-liquid flows were studied to determine the ability of EIT to measure volume-averaged phase fractions. In the liquid-solid tests the mixture was assumed to have properties that varied smoothly over scales much larger than the size of the dispersed solid phase but much smaller than the size of the test vessel. In the air-water bubbly flows, the scale of the dispersed phase (air bubbles) was larger than in the solid-liquid mixture but still small compared to the scale of the apparatus. This represents a progression toward the application of EIT to industrial-scale multiphase flows.

Liquid conductivity in these tests was selected to ensure that resistive effects would dominate over capacitive effects in EIT

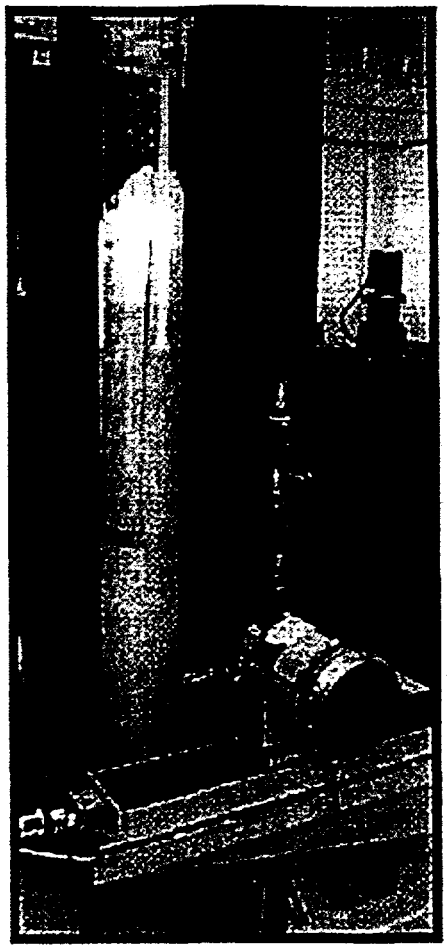

Figure 3. Sandia GDT system shown with the transparent bubble column.

measurements. Controlled amounts of sodium chloride were added to deionized water to obtain the desired conductivity. For resistance to dominate the medium impedance, the following constraint must be satisfied:

$$\sigma_L >> 2\pi f \tilde{\varepsilon} \varepsilon_0 \qquad (3)$$

where f is the AC frequency, $\tilde{\varepsilon}$ is the normalized permittivity (or dielectric constant) of water, and ε_0 is the permittivity of a vacuum. For f = 50 kHz in water, this constraint is satisfied if $\sigma_L >> 2$ μS/cm. Experimental conductivities were chosen to be at least one hundred times higher than this value and were adjusted to compensate for the different impedances of strip and point electrodes.

Solid-liquid experiments. The first comparisons of GDT and EIT (Shollenberger *et al.*, 1997b) involved a closed container of conducting liquid with a flow of insulating particles. Schematic diagrams of the experimental setup are shown in Fig. 4. The testbed was created from the 16-point electrode cylinder, which was capped at

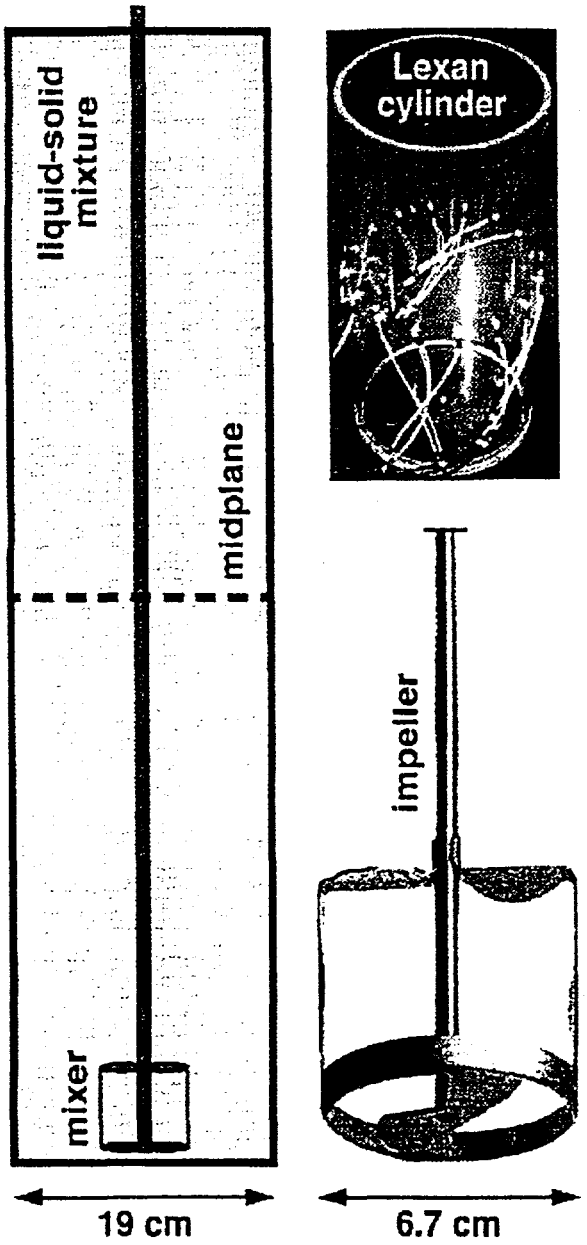

Figure 4. Schematic of test geometry for the liquid-solid experiments showing the EIT electrodes and impeller geometry.

the bottom and the top. A Sargent-Welch mixer was inserted into the cylinder to stir the contents and generate a relatively uniform solids distribution throughout most of the flow inside the cylinder. The mixer system consisted of a compact impeller assembly positioned 1 cm above the lower cylinder cap, a motor mounted above the testbed, and a shaft of 0.8-cm diameter connecting the impeller to the motor. The shaft passed through a small center hole in the top cap of the cylinder around which an "overflow" volume was placed to ensure the absence of free-surface effects — *e.g.*, a vortical "funnel" — in the cylinder interior during mixing.

Deionized water with a known amount of dissolved sodium chloride was chosen for the liquid phase. For the solid phase, glass spheres with a mean diameter of 80 μm were used. Glass is an insulator with respect to salt water, and because of its higher density, glass attenuates gamma photons more strongly than water; these properties make it possible for both EIT and GDT to discriminate between the solid and liquid phases. Glass spheres are also rugged and can easily be separated from water by settling. Variations in the local solids density during mixing were on a scale much larger than the 80-μm diameter of the particles themselves; this provided a smoothly varying phase distribution.

To obtain a nominal cylinder-averaged solid volume fraction ε_S^{NOM}, the required mass of spheres was computed from the volume of the cylindrical testbed, the volume of the spheres, and the known density of the glass. This mass was introduced into the testbed, and water was added to fill the remaining volume. A mixer speed of 600 rpm was applied for 30 minutes to all solid loadings, and a roughly uniform distribution of particles was observed visually within the liquid during measurements. For solid volume fractions much in excess of 0.03, large fluctuating motions and variations in solids distribution could be visually detected, so this study was restricted to values of ε_S^{NOM} no larger than about 0.03 (some solid volume fraction variations were discernible, even at this loading).

The presence of the mixer shaft posed problems for both reconstruction techniques. For GDT it produced extra attenuation when the gamma beam passed through the testbed centerline. These anomalous points were not used in performing the reconstruction. For EIT, placing a good conductor in the center of the testbed would significantly distort the electric field lines, so the steel shaft and impeller were coated with a layer of insulating paint to mitigate this effect. The presence of a small-diameter, axisymmetric, insulated inclusion was expected to have only a small effect on the electrical behavior of the system; EIT measurements with and without the mixer shaft in place, with no particles present, verified this assumption.

For each test condition EIT voltage measurements were repeated during mixing over a span of ten minutes, for a total of 6400 measurements at each electrode. GDT measurements were also taken during mixing for another four minutes. Mixing was then terminated, and the spheres were allowed to settle to the bottom of the water-filled cylinder, a process that was completed after five minutes. Following this settling period EIT was applied again. The second EIT measurement was necessary for calibration purposes because the conductivity of the water was altered by soluble contaminants introduced as the spheres were added. Although these trace contaminants had a negligible effect on GDT, their effect on the water conductivity was comparable to that of the suspended solid particles during mixing.

Table 1 summarizes the measurements by GDT and EIT for three different solid volume fractions. Analysis of the GDT data demonstrated that the radial solids profiles were relatively uniform, as desired. The ratio of the cylinder-averaged mixture gamma attenuation coefficient $\bar{\mu}$ to the liquid attenuation coefficient μ_L was found to increase monotonically with the nominal solid volume fraction ε_S^{NOM}; similarly the ratio of the average mixture conductivity to the liquid conductivity, $(\bar{\sigma}/\sigma_L)$, decreased monotonically with increasing ε_S^{NOM}. By assuming a spatially uniform gamma attenuation coefficient, GDT

Table 1. Comparison of nominal solid volume fractions and values measured by GDT and EIT in the liquid-solid experiment.

ε_S^{NOM}	$\bar{\mu}/\mu_L$	ε_S^{GDT}	$\bar{\sigma}/\sigma_L$	ε_S^{EIT}
0.010	1.015	0.011	0.982	0.012
0.020	1.030	0.021	0.968	0.021
0.030	1.057	0.040	0.940	0.041

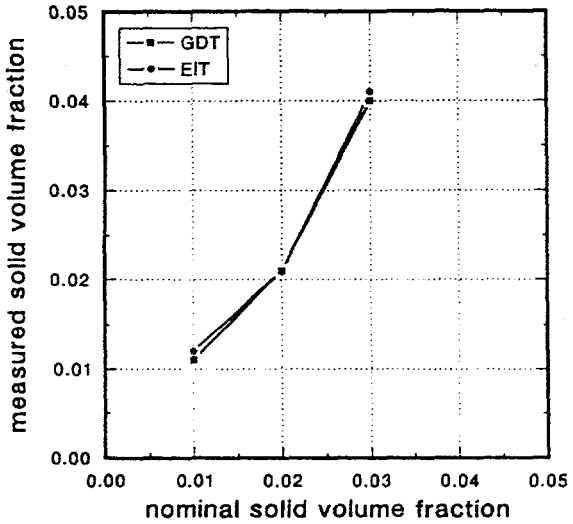

Figure 5. Comparison of solid volume fractions measured by EIT and GDT.

data were converted to a cylinder-average, solid volume fraction ε_S^{GDT} through the formula

$$\varepsilon_S^{GDT} = \frac{\bar{\mu} - \mu_L}{\mu_S - \mu_L} \tag{4}$$

where the attenuation coefficients of the water and glass spheres were previously measured. The three-dimensional Maxwell relation was used to transform EIT data to an average solid volume fraction ε_S^{EIT}:

$$\varepsilon_S^{EIT} = \frac{1 - (\bar{\sigma}/\sigma_L)}{1 + \frac{1}{2}(\bar{\sigma}/\sigma_L)} \tag{5}$$

The conductivity distribution was assumed to be uniform across the domain.

The solid volume fractions determined by GDT and EIT are seen to be in close agreement with each other for all cases (see Fig. 5) and with the nominal values for the first two cases. The case of ε_S^{NOM} = 0.03 is interesting in that the GDT and EIT values are in agreement with each other but are somewhat higher than the nominal value. The mixing was not strong enough to produce a uniform axial distribution of glass spheres throughout the cylinder in this case; the solid volume fraction was less than the nominal value near the top of the cylinder and larger than nominal toward the bottom.

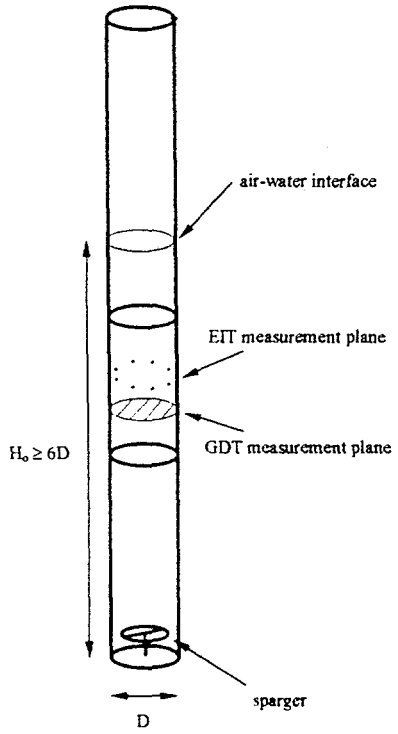

Figure 6. Schematic diagram of air-water bubble column used for EIT and GDT comparisons.

Liquid-gas experiments. Liquid-gas tests of the EIT system were conducted in a transparent bubble column assembled at Sandia as a testbed for optical, electrical, and radiation-based multiphase flow diagnostics (Torczynski *et al.*, 1997). The Lexan column, shown schematically in Fig. 6, has an inner diameter D of 19.05 cm, a wall thickness of 0.64 cm, and is built from interchangeable sections so that different diagnostic tools can be placed in the column. In this study the EIT electrode sections were placed near the center of the column. The point electrodes formed a plane at a distance L of 109.86 cm above the column base, whereas the 16 strip electrodes were centered on a plane L = 97.16 cm above the base. The column was filled with water to a depth H_o of 1.45 m, for a height-to-diameter ratio of 7.6; this depth placed the region of EIT sensitivity completely under water. Air can be introduced at flow rates up to 600 L/min through one of several interchangeable spargers at the base of the column. The spargers are electrically isolated to prevent interference with the EIT system. The column operates at ambient conditions, but the water is subject to evaporative cooling as air is bubbled through; the liquid temperature was held constant by active heating to within ±0.2°C during experiments, which limited variations in conductivity with temperature to ±0.3%.

The goal for the air-water tests was to validate EIT in a flow with variations on a larger scale than the liquid-solid flows. First, a nearly

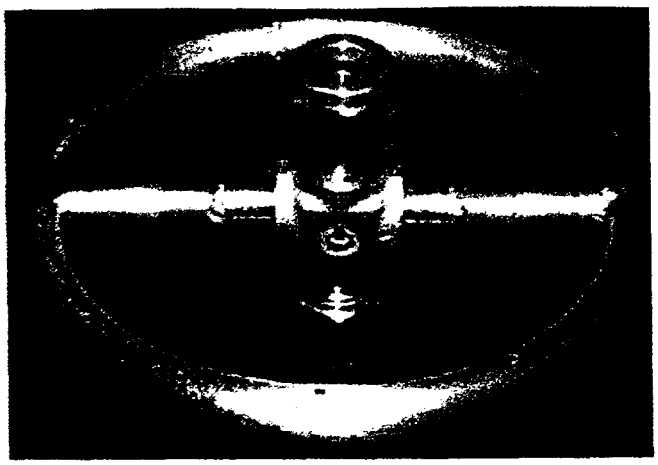

Figure 7. Ring sparger used in churn-turbulent flow experiments.

homogeneous bubbly flow was produced within the column. Two different sparger designs for homogeneous flows were tested, and controlled amounts of surfactant were added to the working liquid to reduce surface tension and prevent coalescence. A truly homogeneous bubbly flow could not be attained with either sparger. GDT reconstructions of the radial gas volume fraction profiles showed a quartic pattern, indicating a low gas volume fraction at the column center from both sparger designs. Vortical motions were also observed at the higher flow rates, indicating a transition from homogeneous to churn-turbulent flow. Next, churn-turbulent flows were examined with EIT and GDT. Such flows in vertical columns normally have parabolic volume fraction profiles that can be reconstructed by both the GDT and EIT algorithms. The sparger used to produce churn-turbulent flows is shown in Fig. 7. This sparger is a hollow stainless steel toroid with a 10.16-cm centerline diameter, an inner tube diameter of 0.95 cm, and ten holes of diameter 0.16 cm facing downward.

For each flow condition 25 full EIT projection sets were averaged to acquire the voltage data for reconstructions; each projection set required less than 0.75 seconds. This averaging was required in order to compare the EIT results with the time-averaged GDT results. The conductivity of the water used in the final liquid-gas experiments was 568±6 μS/cm for point electrode tests and 285±5 μS/cm for strip electrode tests. The source-detector plane of the GDT system was placed to avoid interference from the electrodes. For tests using point electrodes, all gamma paths were in a plane located at L = 96.00 cm above the column base, 13.86 cm below the EIT electrode plane; the measurement chords were parallel and spaced 1 cm apart. During tests with the strip electrodes, GDT measurements were taken in a plane 81.00 cm above the column floor.

Air-water experiments were performed using the ring sparger at five flow rates: 25, 50, 75, 100 and 150 L/min. The corresponding superficial gas velocities ranged from 1.5 to 8.8 cm/s. Figure 8 shows the flow conditions in the column for the minimum and maximum flow rates. At the lowest flow condition, a range of spherical and coalesced nonspherical bubble sizes was evident. A central vortical bubble stream was also seen, similar to the vortical-spiral flow regime described by Chen *et al.* (1994) between dispersed bubbly flows and full turbulence.

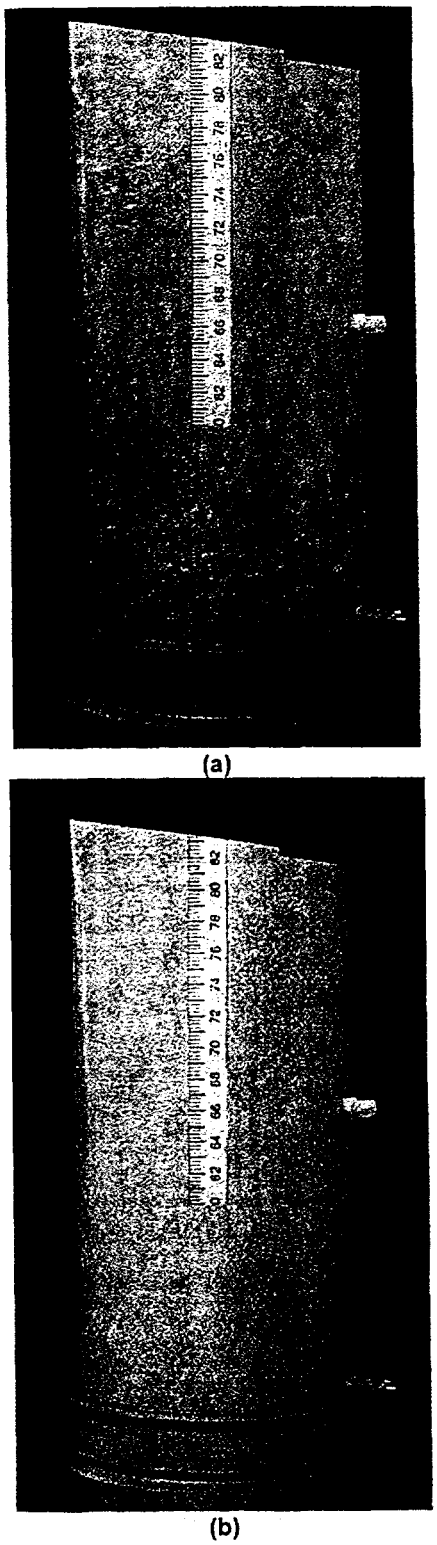

(a)

(b)

Figure 8. Churn-turbulent flow conditions in the transparent bubble column at minimum and maximum flow rates: (a) Q = 25 L/min, (b) Q = 150 L/min.

Table 2. Fundamental EIT voltage solutions for 16 strip electrodes in the transparent bubble column.

Fundamental voltage	Computational value	Experimental value	Experimental value × 1.00688
V_8 (injection)	1.32746	1.23243	1.24091
V_7	0.294654	0.292955	0.294970
V_6	0.145448	0.144345	0.145338
V_5	0.0802970	0.0796277	0.0801754
V_4	0.0443186	0.0439216	0.0442237
V_3	0.0225977	0.0225190	0.0226739
V_2	0.00943046	0.00948088	0.00954609
V_1	0.00227474	0.00229490	0.00231069
V_0 (reference)	0	0	0

At rates of 75 L/min and above, the flow was completely opaque and turbulent to the eye.

As an aid in evaluating the results, the fundamental EIT voltage solutions for an axisymmetric conductivity profile were computed. [The reader is referred to Torczynski *et al.* (1997) for a complete discussion of fundamental voltages.] Because of axisymmetry a complete set of R_V voltage measurements will yield only $N/2$ independent pieces of information in the fundamental solution. The experimental voltages were also reduced to fundamental values for comparison with the computed solutions. The reduced voltages from the point electrodes were in poor agreement with predicted values; at all noninjection, nonground electrodes, the experimental voltages were similar, indicating poor sensitivity to variations in the conductivity profile. Conversely, data measured with the strip electrodes were in excellent agreement with the predicted values and were much more sensitive to the conductivity profile. As seen in Table 2, when a multiplicative factor of 1.00688 is used, the computational and experimental voltages agree to almost three significant figures. A difference of 0.7% in computational and experimental voltages at all electrodes is reasonable, since experimental uncertainty in AC current and liquid conductivity are about 0.5%, and computational accuracy is similar. Based on these results strip electrode data was used exclusively to reconstruct radial profiles of the churn-turbulent flows.

In both the EIT and GDT reconstructions, the radial volume fraction distribution was represented by parametric formulas. The conductivity distribution in EIT reconstructions was assumed to be parabolic across the column, taking the form

$$\frac{\sigma}{\sigma_L} = \frac{1 + c[2(r/R)^2 - 1]}{b} \tag{6}$$

where b is a scale parameter, c is the parabolic shape parameter, and R is the radius of the bubble column. Similarly chord-averaged gas volume fractions computed from GDT data were fit to a second or fourth-order polynomial before the Abel transform was taken. With both EIT and GDT, the column-average gas volume fraction ε_G was determined by analytically averaging the resulting profile over the column area. Figure 9 shows typical gas volume profiles and the column-average gas volume fractions as a function of flow rate, determined from both methods. The EIT profile tends to lie slightly above the GDT profile at each flow rate. The GDT and EIT gas volume fractions are in excellent agreement, however, all lying within 0.01 (absolute volume fraction) of each other at all radial positions, despite variations in the local volume fraction across the column as large as 0.2.

Because of the difference in collection times for the two methods (about 23 minutes for GDT but less than 20 seconds for EIT), it was decided to look for slow cyclic behavior in the flows which might be averaged out by GDT but not by EIT. Separate flow measurements were taken with an impedance-based bulk void fraction meter, shown in Fig. 10. This instrument has two rectangular electrodes 3.8 cm tall, which subtend 120° each on opposite sides of the column. A 50-kHz AC signal is applied to the electrodes, and the voltage across the electrodes may be recorded with a digitizing oscilloscope for analysis. In earlier work this meter was used to measure bulk gas volume fractions through comparisons of signals from flow and no-flow conditions (Torczynski *et al.*, 1997). Here Fourier spectra and signal-to-noise ratios were computed from the recorded voltages to determine the frequencies and magnitudes of void fraction fluctuations.

Voltages were recorded over periods of ten minutes under the same flow conditions as the GDT-EIT tests. Signal spectra revealed no coherent periodic behavior in the flow over the range of zero to 12.5 Hz; this alleviated the concern that EIT measurements were capturing data over only a portion of slow flow cycles. Signal-to-noise ratios at flow and no-flow conditions, along with the assumption of Gaussian error propagation, were used to compute voltage variations due to flow fluctuations. By correlating mean voltages with average gas volume fractions, variations in ε_G over the course of the measurement were thus estimated. Table 3 presents the estimated fluctuations at each flow rate; except for the lowest flow rate, fluctuations are higher than the discrepancy between EIT and GDT, again suggesting that both methods are incorporating such variations in their measurements.

In summary, the EIT system has been validated for measurement of solid volume fractions in solid-liquid flows, and gas volume fractions and radial profiles in gas-liquid flows. Future work will include the measurement of gas-liquid-solid flows in the bubble column to examine the effect of the solid phase on hydrodynamic behavior. The study will employ a solid phase with conductive properties similar to air and a density similar to water, so that EIT will detect both the solid and gas phases but gamma attenuation will only be influenced by air, as before. The difference in the radial profiles from the GDT and EIT reconstructions will yield the radial solids distribution in the three-phase flow. The solid volume fraction in these three-phase tests will be well above 0.01, based on the difference in gas volume fraction results from two-phase tests.

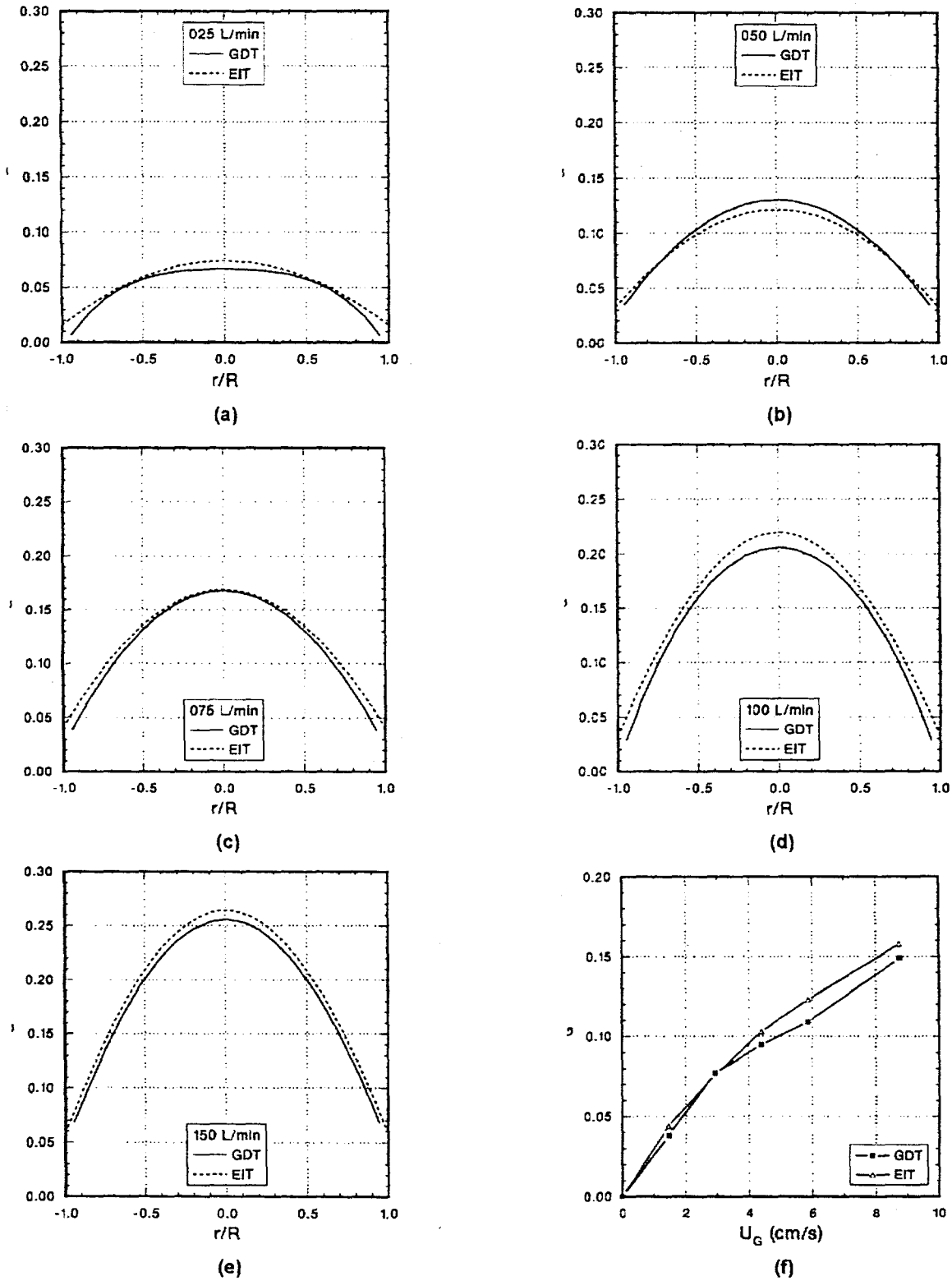

Figure 9. Comparisons of gas volume fraction measurements from GDT and EIT. Figures (a) through (e) are radial profiles measured at the indicated flow rates; (f) presents column average gas volume fractions for all flow rates.

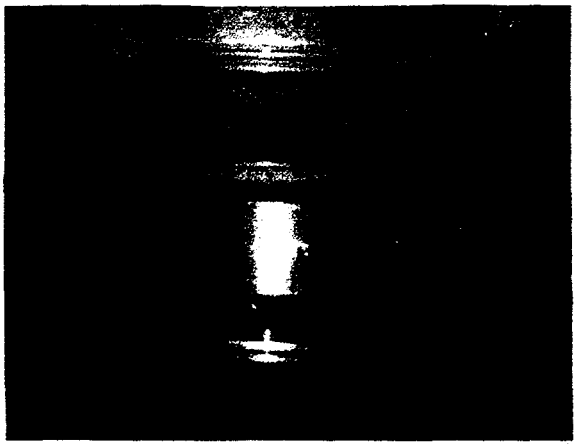

Figure 10. Impedance-based bulk void fraction meter used to investigate fluctuations in gas volume fraction.

Table 3. Maximum fluctuations in gas volume fraction as measured by the bulk void fraction meter.

U_G (cm/s)	ε_G	maximum $\Delta\varepsilon_G$
1.5	0.038	0.006
2.9	0.076	0.014
4.4	0.094	0.015
5.9	0.109	0.018
8.8	0.148	0.051

CONCLUSIONS

Researchers continue to make significant advances in applying tomographic techniques to multiphase flows. Tomography systems are being developed specifically to study multicomponent flows, and improvements in temporal and spatial resolution are a continuing goal. The case study described above demonstrates how quantitative phase distribution data can be derived from nonintrusive measurements. Researchers are striving to develop systems with reduced cost and increased flexibility for use in the field. In the future multiphase flow tomography will become available for use in both the laboratory and in actual industrial processing.

REFERENCES

Abbott, J. R., Tetlow, N., Graham, A. L., Altobelli, S. A., Fukushima, E., Mondy, L. A., and Stephens, T. S., 1991, "Experimental Observations of Particle Migration in Concentrated Suspensions: Couette Flow," *Journal of Rheology*, Vol. 35, pp. 773-795.

Adkins, D. R., Shollenberger, K. A., O'Hern, T. J., and Torczynski, J. R., 1996, "Pressure Effects on Bubble Column Flow Characteristics," *ANS Proceedings of the 1996 National Heat Transfer Conference*, American Nuclear Society, LaGrange Park, IL, THD-Vol. 9, pp. 318-325.

Altobelli, S., Givler, R. C., and Fukushima, E., 1991, "Velocity and Concentration Measurements of Suspensions by Nuclear Magnetic Resonance Imaging," *Journal of Rheology*, Vol. 35, pp. 721-734.

Altobelli, S., and Mondy, L., 1998, "Hindered Flotation Functions from NMR Imaging," submitted for publication in *Physics of Fluids*.

Beck, M. S., Campogrande, E., Morris, M., Williams, R. A., and Waterfall, R. C., eds., 1993, *Tomographic Techniques for Process Design and Operation*, Computational Mechanics Publications, Southampton.

Ceccio, S. L., and George, D. L., 1996, "A Review of Electrical Impedance Techniques for the Measurement of Multiphase Flows," ASME *Journal of Fluids Engineering*, Vol. 118, pp. 391-399.

Chen, R. C., Reese, J., and Fan, L.-S., 1994, "Flow Structure in a Three-Dimensional Bubble Column and Three-Phase Fluidized Bed," *AIChE Journal*, Vol. 40, pp. 1093-1104.

Dickin, F. J., Williams, R. A., and Beck, M. S., 1993, "Determination of Composition and Motion of Multicomponent Mixtures in Process Vessels using Electrical Impedance Tomography - I. Principles and Process Engineering Applications," *Chemical Engineering Science*, Vol. 48, pp. 1883-1897.

Dyakowski, T., 1996, "Process Tomography Applied to Multi-Phase Flow Measurement," *Measurement Science and Technology*, Vol. 7, pp. 343-353.

Fluid Dynamics International, 1995, *FIDAP Users Manual*, Fluid Dynamics International, Evanston, IL.

George, D. L., Ceccio, S. L., Shollenberger, K. A., Torczynski, J. R., and O'Hern, T. J., 1998, "Comparison of Electrical-Impedance Tomography and Gamma-Densitometry Tomography for the Measurement of Gas Volume Fraction Profiles in a Bubble Column," *Proceedings of the 1998 ASME Fluids Engineering Division Summer Meeting*, FED-Vol. 245, No. 98-5081.

Jones, O. C., Lin, J. T., and Ovacik, L., 1992, "Investigation of Electrical Impedance Imaging Relative to Two-Phase, Gas-Liquid Flows," *Chemical Engineering Communications*, Vol. 118, pp. 299-325.

Jones, O. C., Lin, J. T., Ovacik, L., and Shu, H., 1993, "Impedance Imaging Relative to Gas-Liquid Systems," *Nuclear Engineering and Design*, Vol. 141, pp. 159-176.

Jones, O. C., Lin, J. T., Shu, H., Ovacik, L., and He, Y., 1994, "Impedance Imaging Relative to Binary Mixtures," *Fifth International Symposium on Liquid-Solid Flows*, ASME, Lake Tahoe, NV.

Kose, K., 1992, "Visualization of Turbulent Motion using Echo-Planar Imaging with a Spatial Tagging Sequence," *Journal of Magnetic Resonance*, Vol. 98, pp. 599-606.

Larachi, F., Kennedy, G. and Chaouki, J., 1994, "A γ-Ray Detection System for 3-D Tracking in Multiphase Reactors," *Nuclear Instruments and Methods*, Vol. A338, pp. 568-576.

Lin, J. S., Chen, M. M., and Chao, B. T., 1985, "A Novel Radioactive Particle Tracking Facility for Measurements of Solids Motion in Gas Fluidized Beds," *AIChE Journal*, Vol. 31, pp. 465-473.

Maxwell, J. C., 1881, *A Treatise on Electricity and Magnetism*, Clarendon Press, Oxford.

McKee, S. L., Williams, R. A., and Boxman, A., 1995, "Development of Solid-Liquid Mixing Models using Tomographic Techniques," *Chemical Engineering Journal*, Vol. 56, pp. 101-107.

Munshi, P., 1990, "A Review of Computerized Tomography with Applications to Two-Phase Flows," *Sadhana*, Vol. 15, Part 1, pp. 43-55.

O'Hern, T. J., Torczynski, J. R., Ceccio, S. L., Tassin, A. L., Chahine, G. L., Duraiswami, R., and Sarkar, K., 1995, "Development of an Electrical-Impedance Tomography System for an Air-Water

Vertical Bubble Column," *ASME Forum on Measurement Techniques in Multiphase Flows*, T. J. O'Hern, A. Naqwi, C. Presser, and R. D. Skocypec, eds., American Society of Mechanical Engineers, New York, FED-Vol. 233, pp. 531-537.

Parker, D. J., Hawkesworth, M. R., Beynon, T. D., and Bridgwater, J., 1993, "Process Engineering Studies Using Positron-Based Imaging Techniques," *Tomographic Techniques for Process Design and Operation*, Beck, M. S., Campogrande, E., Morris, M., Williams, R. A., and Waterfall, R. C., eds., Computational Mechanics Publications, Southampton, pp. 239-250.

Parker, D. J., Hawkesworth, M. R., and Beynon, T. D., 1995, "Process Applications of Emission Tomography," *Chemical Engineering Journal*, Vol. 56, pp. 109-117.

Plaskowski, A., Beck, M. S., Thorn, R., and Dyakowski, T., 1995, *Imaging Industrial Flows: Applications of Electrical Process Tomography*, Institute of Physics Publishing, Bristol.

Powell, R. L., 1998, "Studies of Pulp Suspensions Using Nuclear Magnetic Resonance Imaging (NMRI)," *Proceedings of the 1998 ASME Fluids Engineering Division Summer Meeting*, FED-Vol. 245, No. 98-5072.

Roy, S., Chen, J., Degaleesan, S., Gupta, P., Al-Dahhan, M. H., and Dudukovic, M. P., 1998, "Non-Invasive Flow Monitoring in Opaque Multiphase Reactors via CARPT and CAT," *Proceedings of the 1998 ASME Fluids Engineering Division Summer Meeting*, FED-Vol. 245, No. 98-5077.

Shekarriz, A. and Brenden, B. B., 1995, "Planar Ultrasonic Imaging of a Two-Phase Mixture," *Journal of Fluids Engineering*, Vol. 117, pp. 317-319.

Shekarriz, A., Brenden, B. B., and Kytomaa, H. K., 1998, "Planar Ultrasound Technique for Real-Time Visualization and Concentration Measurements in Dense Solid-Liquid Slurries," *Proceedings of the 1998 ASME Fluids Engineering Division Summer Meeting*, FED-Vol. 245, No. 98-5226.

Shollenberger, K. A., Torczynski, J. R., Adkins, D. R., O'Hern, T. J., and Jackson, N. B., 1997a, "Gamma-Densitometry Tomography of Gas Holdup Spatial Distribution in Industrial-Scale Bubble Columns," *Chemical Engineering Science*, Vol. 52, pp. 2037-2048.

Shollenberger, K. A., Torczynski, J. R, O'Hern, T. J., Adkins, D. R., Ceccio, S. L., and George, D. L., 1997b, "Comparison of Gamma-Densitometry Tomography and Electrical-Impedance Tomography for Determining Material Distribution in Liquid-Solid Flows," *Proceedings of the 1997 ASME Fluids Engineering Division Summer Meeting*, J. Katz and K. J. Farrell, eds., American Society of Mechanical Engineers, New York, Vol. FEDSM '97, No. 97-3690.

Simons, S. J. R., 1995, "Imaging Techniques for Fluidized Bed Systems: a Review," *Chemical Engineering Journal*, Vol. 56, pp. 83-93.

Torczynski, J. R., O'Hern, T. J., Shollenberger, K. A., Ceccio, S. L., and Tassin, A. L., 1996a, "Finite Element Method Electrical Impedance Tomography for Phase Distribution Determination in Multiphase Flows: Validation Calculations and Experiments," ASME Cavitation and Multiphase Flow Forum, J. Katz and K. J. Farrell, eds., American Society of Mechanical Engineers, New York, FED-Vol. 236, pp. 497-501.

Torczynski, J. R., Adkins, D. R., Shollenberger, K. A., and O'Hern, T. J., 1996b, "Application of Gamma-Densitometry Tomography to Determine Phase Spatial Variation in Two-Phase and Three-Phase Bubbly Flows," *ASME Cavitation and Multiphase Flow Forum*, J. Katz and K. J. Farrell, eds., American Society of Mechanical Engineers, New York, FED-Vol. 236, pp. 503-508.

Torczynski, J. R., O'Hern, T. J., Adkins, D. R., Jackson, N. B., and Shollenberger, K. A., 1997, *Advanced Tomographic Flow Diagnostics for Opaque Multiphase Fluids*, Report SAND97-1176, Sandia National Laboratories, Albuquerque, NM.

Vest, C. M., 1985, "Tomography for Properties of Materials that Bend Rays: a Tutorial," *Applied Optics*, Vol. 24, pp. 4089-4094.

Webster, J. G., ed., 1990, *Electrical Impedance Tomography*, Adam Hilger, Bristol.

Yates, J. G., and Cheesman, D. J., 1992, "Voidage Variations in the Regions Surrounding a Rising Bubble in a Fluidized Bed," *AIChE Symposium Series*, Vol.88, pp. 34-39.

Yorkey, T. J., Webster, J. G., and Tompkins, W. J., 1987, "Comparing Reconstruction Methods for Electrical Impedance Tomography," *IEEE Transactions on Biomedical Engineering*, Vol. 11, pp. 843-852.